Lithos 112S (2009) 1155–1166

Contents lists available at ScienceDirect

Lithos

journal homepage: www.elsevier.com/locate/lithos

The lithospheric mantle below southern West Greenland: A geothermobarometric approach to diamond potential and mantle stratigraphy

Karina K. Sand [a,*], Tod E. Waight [b], D. Graham Pearson [c], Troels F.D. Nielsen [a], Emil Makovicky [b], Mark T. Hutchison [a]

[a] Geological Survey of Denmark and Greenland, Øster Voldgade 10, 1350 Copenhagen K, Denmark
[b] Institute for Geography and Geology, University of Copenhagen, Denmark. Øster Voldgade 10, 1350 Copenhagen K, Denmark
[c] Northern Centre for Isotopic and Elemental Tracing, Department of Earth Sciences, Durham University, Science Labs, Durham DH1 3LE, United Kingdom

ARTICLE INFO

Article history:
Received 5 October 2008
Received in revised form 23 April 2009
Accepted 17 May 2009
Available online 13 June 2009

Keywords:
Geothermobarometry
Diamond potential
Greenland
Mantle
Lithosphere
Peridotite

ABSTRACT

Geothermobarometry of primarily garnet lherzolitic xenoliths from several localities in southern West Greenland is applied to address the diamond potential, pressure and temperature distribution and the stratigraphy of the subcontinental lithospheric mantle ~600 Ma ago. The samples are from kimberlitic and ultramafic lamprophyre (senso lato) dikes and sills emplaced into three tectonically distinct crustal areas in the North Atlantic Craton. Several geothermobarometry formulations have been applied and a thorough assessment of which *P–T* combinations are most applicable to this sample suite has been conducted. No variation in *P–T* gradients between the three distinct crustal areas has been discerned. We find that the lithospheric mantle beneath this region extended to a depth of 215 km at the time of eruption, with a geotherm similar to those defined by peridotites from the Slave craton and the Kirkland Lake locality within the Superior craton. In supporting previous studies we find that the continental lithospheric mantle is layered and increases in fertility with depth. Twenty-five of 32 investigated samples are estimated to be derived from the diamond stability field that extends into the reworked Archean North of the Naqssugtoqidian deformation front.

1. Introduction

In recent years the number of diamond finds in ultramafic lamprophyres (UML's) and spatially related kimberlitic rock types from southern West (SW) Greenland has increased (Nielsen and Sand, 2008; Hutchison and Heaman, 2008), resulting in a greater interest in the diamond potential of the region. This renewed interest has resulted in many new discoveries of in-situ kimberlitic dikes and sheets, from which our working group has collected over 200 mantle xenoliths. The petrography, bulk composition and groundmass phases and genesis of UML magma types in SW Greenland is complex and variable (Nielsen et al., this issue; Nielsen and Sand, 2008) and the reader is referred to a discussion of these topics based on similar UML magmas encountered in the Torngat region, Labrador, Canada (Tappe et al., 2008). Additional information on the kimberlitic rocks of SW Greenland is given in Larsen and Rex (1992), while Jensen et al. (2003, 2004) provide comprehensive lists of relevant publications, reports and locality descriptions.

The xenolith-bearing occurrences included in this study (Fig. 1) are located in three different tectonic settings (Kangerlussuaq, Sarfartoq and Maniitsoq) relative to the margin of the Archean North Atlantic craton. Bizzarro and Stevenson (2003) and Bernstein et al. (1998) have shown that the subcontinental lithospheric mantle (SCLM) beneath this region is highly depleted, with dunite being a common lithology. The dunites have experienced extensive (>40%) shallow melting, possibly in an arc setting, before evolving into the SCLM (Pearson and Wittig, 2008; Wittig et al., 2008). Previous thermobarometry investigations on xenoliths from these areas comprise the work by Garrit et al. (1996), Garrit (2000), Bizzarro and Stevenson (2003), Griffin et al. (2004), Sand (2007) and Hutchison and Frei (this issue). Garrit et al. (1996) and Garrit (2000) constructed mantle lithology sections for the Maniitsoq and Sarfartoq areas and investigated the proportion of garnet types with depth based on circa 65 xenoliths and 17 garnet concentrates from kimberlites and UML. The mantle sections obtained comprised different proportions of mantle lithologies, though both areas were suggested to be dominated by lherzolite with lenses of harzburgite and wehrlite (Garrit, 2000). Bizzarro and Stevenson (2003) based their work on 10 mantle xenoliths from two dykes in the Sarfartoq area. They interpreted the lithospheric mantle to consist of two layers: an upper depleted layer (70–180 km) consisting of coarse refractory peridotites, and a lower layer (180–225 km) characterized by fertile clinopyroxene-bearing porphyroclastic garnet-lherzolites. Hutchison and Frei (this issue) used *P–T* data for 5 xenoliths to demonstrate that the mantle

* Corresponding author. Present address: Nano-Science Center, Department of Chemistry, University of Copenhagen, Universitetsparken 5, 2100 Copenhagen Ø, Denmark. Tel.: +45 35320232; fax: +45 35320214.
E-mail address: karina.sand@gmail.com (K.K. Sand).

0024-4937/$ – see front matter © 2009 Elsevier B.V. All rights reserved.
doi:10.1016/j.lithos.2009.05.012

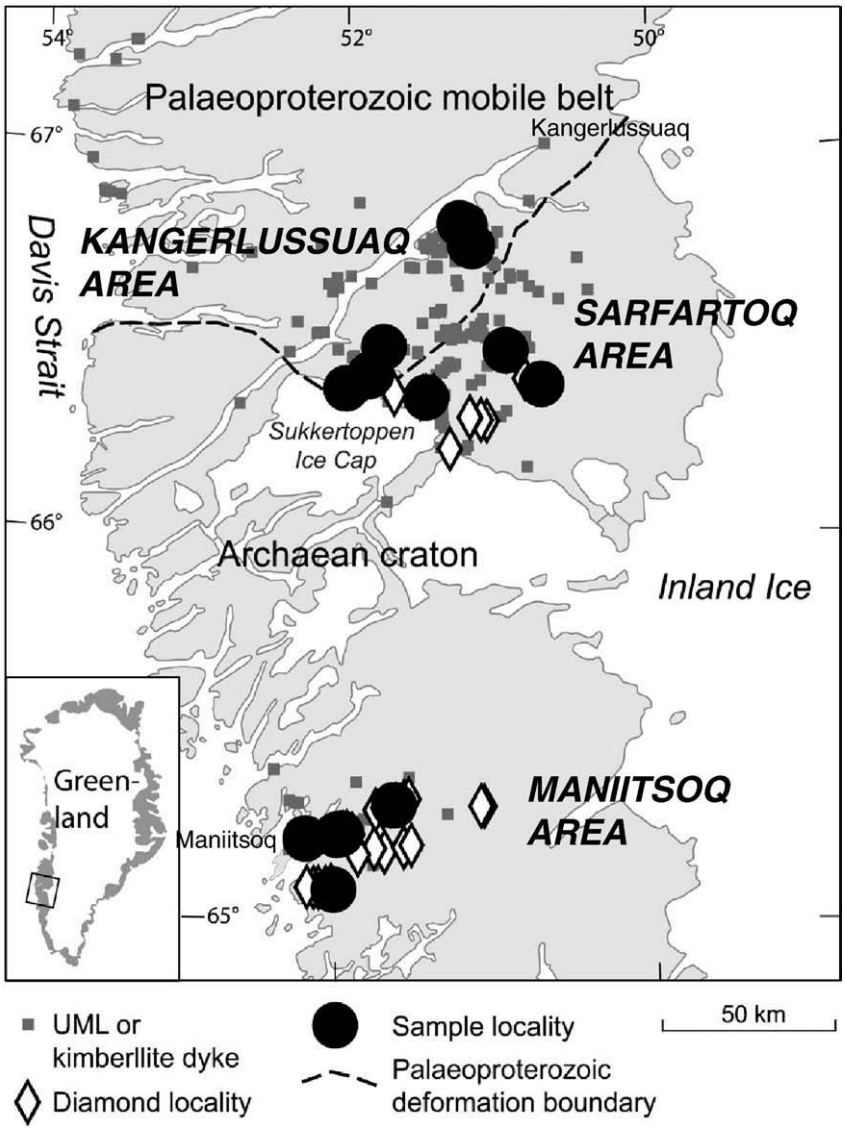

Fig. 1. Map of the study area showing the localities of the *P–T* results presented here, and the in-situ occurrences of kimberlitic and ultramafic lamprophyre in the three main kimberlite fields: Maniitsoq, Sarfartoq, and Kangerlussuaq. The boundary between the Sarfartoq and Kangerlussuaq areas are given by the deformation boundary.

lithosphere below Garnet Lake (Sarfartoq area) at the time of sampling in the late Neoproterozoic was relatively cool, with a 41 mW/m^2 model-conductive geotherm and a depth of ~200 km.

The work presented here is based on data from Sand (2007) and expands on the previous studies by examining a considerably larger collection of four- and three-phase mantle xenoliths. We aim to provide robust *P–T* estimates for mantle material from the Kangerlussuaq, Sarfartoq and Maniitsoq regions and thereby outline a xenolith-based perspective of the lithospheric stratigraphy. In addition to diamond potential, structure and thickness of the subcontinental lithospheric mantle (SCLM) a thorough comparison of different geothermobarometry formulations has been conducted within the context of the SW Greenland peridotite suite. The new results indicate that the choice of barometer–thermometer can greatly influence modeled geothermal conditions in this area, as found for other cratonic regions (Finnerty and Boyd, 1987). Rigorous testing by Sand (2007) established the geothermobarometer pair of PMC and TCa-in-opx as most likely to yield *P–T* results closest to true ambient conditions for similar xenoliths from West Greenland. In this work we propose use of a different preferred geothermobarometer combination. Table 1 lists the abbreviations for minerals, rock types and mantle thermobarometers etc. used in this work.

2. Regional geology

The investigated samples were collected from the northern and central part of the Archean North Atlantic craton and across the tectonic boundary into the southern extension of the Nagssugtoqidian orogen (Fig. 1). The former is undeformed by post-Archaean events and the latter consists mainly of Archean rocks reworked during the 1.8–1.95 Ga orogeny which comprised south-dipping subduction (van Gool et al., 1999). Our work focuses on the Kangerlussuaq, Sarfartoq, and Maniitsoq areas that form an approximately north–south traverse across the region. The Kangerlussuaq area falls to the north of the deformation front and is dominated by Archean amphibolite-facies gneisses, reworked during the Nagssugtoqidian orogeny (van Gool et al., 2002). The hypabyssal intrusions that host xenoliths in this area are generally less than 60 cm, and rarely more than 1 m, wide. Due to the gentle topography the sills and dykes can rarely be followed in-situ for more than 50 m. The Sarfartoq area, occurring immediately south of the orogenic front, comprises granulite-facies orthogneisses and paragneisses that are cut by generally undeformed Archean granitiods. The geological occurrence of kimberlitic rock types is similar to the Kangerlussuaq area. This area also hosts the Sarfartoq carbonatite complex, recently dated to 564 Ma and emplaced (pene)

Table 1
Common mineral, rock type, thermobarometry and other abbreviations.

SCLM	Subcontinental lithospheric mantle
Cpx, cpx	Clinopyroxene
Dia, dia	Diamond
Gph, gph	Graphite
Grt, grt	Garnet
Ol, ol	Olivine
Sp, sp	Spinel
Opx, opx	Orthopyroxene
G10, G9 etc.	Garnet classifications according to Grütter et al. (2004)
Lhz	Lherzolite (Ol + Opx + Cpx assemblage)
Hzb	Harzburgite (Ol + Opx assemblage, no Cpx)
Weh	Wehrlite (Ol + Cpx assembalge, no Opx)
Dun	Dunite (>90% Ol assemblage)
Ma, Ga	10^6, 10^8 years
P	Pressure in kilobar (kbar) or GigaPascal (GPa)
T	Temperature, in degrees Celsius (°C)
TBKN	Cpx–Opx solvus thermometer of Brey and Köhler (1990)
TCa-in-opx	Brey and Köhler (1990)
THarley	Fe–Mg exchange between grt and opx. Harley (1984)
TNT	Enstatite-in-Cpx thermometer of Nimis and Taylor (2000)
TO´Neill	Fe–Mg exchange between grt and ol. O`Neill and Wood (1979)
PBKN	(Al,Cr)Opx + Grt barometer of Brey and Köhler (1990)
PMC	Al-Opx + Grt barometer as formulated by Finnerty and Boyd (1984)
PNG	(Al,Cr)Opx + Grt barometer of Nickel and Green (1985)
PNT	(Al,Cr)Cpx + Grt barometer of Nimis and Taylor (2000)
CPL	Crossed polarized light
PPL	Plane polarized light
BSE	Backscatter electron image

contemporaneously with the kimberlitic dikes and sills 555–604 Ma ago (Secher and Larsen, 1978; Secher and Larsen, 1980; Hutchison and Heaman, 2008; Secher et al., this issue). The Maniitsoq area is located centrally within the exposed SW Greenland craton and comprises Archean tonalitic and granodioritic gneisses (Kalsbeek, 1976; Wedepohl et al., 1991). In this area the kimberlitic dykes generally dip steeply and form a WSW–ENE striking dyke system (Jensen et al., 2005). The dykes are generally between 0.5 and 1 m wide and can be followed for several hundred meters to kilometers. Mantle xenoliths of harzburgite and dunite were found at many of the circa 30 individual xenolith localities investigated, and were found to dominate the xenolith suites at the craton edge. Lherzolite xenoliths are much more prevalent in the Maniitsoq area, where wehrlites are also common. Here we focus largely on the garnet lherzolite xenoliths because of their amenability to thermobarometry.

3. Methodology

3.1. Petrology

Mineral modes were estimated visually from standard petrographic thin sections and are used for the classification and naming of the mantle lithologies. Modes calculated from bulk compositions for 24 large samples are presented in Wittig et al. (2008) along with major and trace elements (Table 2). All samples were characterized with respect to mineral textures and alteration parageneses. The petrographic classification of mantle xenoliths used in this study is based on the primary mineralogy where lherzolite vs. harzburgite is defined by the observed presence or absence of clinopyroxene. The textural classification for peridotites used here is adopted from Harte (1977). Metasomatic events and their effects on mineral composition and equilibrium relationships are interpreted based on petrographic observations and major element compositions determined by electron microprobe. We distinguish between primary and secondary metasomatism where the former precedes the entrainment of the peridotites in the kimberlitic melt. Secondary metasomatism occurs during the upward movement towards the surface and, for our purposes, includes surficial low-temperature weathering. Table 2 provides a comprehensive summary of characteristics for the 42 new xenoliths investigated.

3.2. Analytical methods

Minerals were analysed using a JEOL 8200 electron microprobe housed at the Institute of Geography and Geology, Copenhagen, Denmark. Acceleration voltage was 15 kV and beam current 50 nA and beam diameter 5 µm. Measurements were performed with WDS using counting times of 20 s on peak and 20 s on background. Individual grains were measured several times and a minimum of four grains of each mineral species in each sample were analysed. Four to five spots in the core region and four to five spots in the rim of each crystal were analysed in pyroxene and olivine grains. Garnets were analysed with ~10 spots in the cores and ~10 spots in the rims where possible. The variation of replicate analyses was greater than the reproducibility in 1–2 grains for 4 of the 42 xenoliths investigated. These variations were all non-systematic and the grains were accordingly considered to be compositionally heterogeneous and were rejected for *P–T* analysis as they are likely to represent secondary alteration. The compositional data presented in online Supplementary Table B and used for geothermobarometry represent averages of multiple analyses. This statistically and time consuming approach to mineral homogeneity was chosen based on a test assessing the effects on the *P–T* estimates where the sample mean has a 2σ greater than the estimated reproducibility (Sand, 2007). The test showed that such heterogeneous samples may give rise to uncertainties that exceed those resulting from errors in the experimental calibrations (e.g. ±60 °C, Brey and Köhler, 1990). The typical uncertainties observed in the test for homogeneous samples are well within the overall uncertainty of the geothermometry methods.

3.3. Geothermobarometry

In order to obtain information on ambient mantle conditions from geothermobarometry, it is crucial that the mineral parageneses are equilibrated. To evaluate attainment of equilibrium between phases in our samples the following criteria are used (after Finnerty and Boyd (1984) and Vernon, 2004): a) absence of disequilibrium textures, e.g. vermicular crystal shapes, dissolution or exsolution textures. b) A consistent element distribution between coexisting phases. c) Mineral homogeneity at thin section scale. d) Consistent *P–T* estimates from different geothermobarometers based on several exchange reactions. In Sections 4.1 and 4.2 of this work we show that 24 samples accepted for *P–T* work comply with criteria (b) and (c), though we discuss in more detail the fulfillment of criterion (a) for clinopyroxene in Section 5.3.

The normal procedure of assuming that $Fe^{2+} = Fe^{total}$ for garnets, olivine and pyroxene (e.g. Finnerty and Boyd, 1984; Pearson, 2003; Smith, 1999) is adopted while realizing that the presence of Fe^{3+} will have some effect on the resulting *P–T* estimates. Canil and O`Neill (1996) have suggested that the presence of Fe^{3+} may result in calculated temperature differences of up to 200 °C. *P–T* calculations are here made using a combination of the PTXL and PTEXL macros written by Dr. Thomas Köhler and a spreadsheet made by Ian Fitzsimons of Curtin University in Australia in 1995. The latter spreadsheet was modified to incorporate all the thermobarometers used in this study.

4. Results

Petrographic studies were completed on a total of 81 mantle peridotite samples that represent circa 30 xenolith localities from across the region (Fig. 1; Supplementary Table A). None of the 27 samples selected for more detailed *P–T* work (Table 2) show signs of modal metasomatism, such as the presence of phlogopite, potassic

Table 2
Summary of petrographic and compositional attributes for xenoliths discussed in this work.

Sample	Texture	Ol%	Opx%	Cpx%	Grt%	Spl%	Rock type	Grt type	Ol Mg#	Opx Mg#	Cpx Mg#	Grt Mg#	Remarks	*P–T* subset	Online table B	Wittig et al., 2008
444247	Coarse equant to porphyroclastic	80	5	10	5	0	Grt lhz	G9	90.45	91.03	90.85	78.37	Cpx is lobate with turbid alteration rims. Grt heterogeneous in Cr	Discarded	Yes	No
464637d	Coarse tabular	83	5	5	2	0	Grt lhz	G9	88.64	90.22	89.10	77.61	Kimberlite infiltration. Cpx is lobate with turbid alteration rims.	Yes	Yes	No
474527	(Coarse tabular to) porphyroclastic	80	10	5	5	0	Grt lhz	G9	91.96	92.86	91.90	84.12	Cpx is lobate with turbid alteration rims. Ol is serp	Yes	Yes	Yes
474540	Coarse tabular	76	7	7	10	0	Grt lhz	G9	92.40	93.34	92.68	85.30	Cpx rims are altered.	Yes	Yes	No
474547	Coarse tabular	85	6	4	4	1	Grt-sp lhz	G9	92.64	93.86	92.68	84.48	Cpx has turbid alteration rims. Rare chromite incl. in cpx	Yes	Yes	Yes
474555	Coarse equant to tabular	65	15	10	10	0	Grt lhz	G9	91.19	92.28	91.16	82.06	Kimberlite infiltration. Cpx has turbid alteration rims.	Yes	Yes	Yes
474556a	Porphyroclastic with disrupted garnets	70	10	5	15	0	Grt lhz	G5	88.33	91.44	90.61	81.55	Strong kimberlitic infiltration. Cpx are lobate with turbid alteration rims.	Yes	Yes	No
474568	Coarse equant to tabular	75	10	5	10	0	Grt lhz	G11	90.70	91.82	90.70	82.52	Cpx is lobate with turbid alteration rims	Yes	Yes	Yes
474570	Porphyroclastic	80	<5	<5	1	0	Grt lhz	G12	n.a.	n.a.	n.a.	n.a.	Few grains of cpx, opx and grt. Little serpentinizaton.	No	No	Yes
4745741	Coarse equant to tabular	>85	<5	<5	5	0	Grt lhz	G9	n.a.	n.a.	n.a.	n.a.	Same rock as below.	No	No	No
474574a	Coarse tabular	>85	10	<1	3	0	Grt lhz	G9	92.74	93.61	92.70	84.20	Kimberlitic infiltration. Cpx has turbid alteration rims.	Yes	Yes	Yes
474575	Coarse equant to weak porphyroclastic	83	5	1	10	0	Grt lhz	G9	90.16	92.34	91.37	82.95	Heavy carbonate rich infiltration	Yes	Yes	Yes
474577	Porphyroclastic to coarse equant	>70	20	<5	5	0	Grt lhz	G9	91.49	92.47	91.86	83.86	Cpx has turbid alteration rims.	Yes	Yes	Yes
477421	Coarse mosaic = equant	73	20	5	2	0	Grt-sp lhz	G9	91.72	92.80	92.37	80.76	Kimberlitic infiltration. Cpx has turbid alteration rims.	Yes	Yes	Yes
481842	Coarse tabular	75	10	5	10	0	Grt lhz	G9	92.34	93.25	92.98	82.67	Cpx lobate to indented	Yes	Yes	No
483806c1	Coarse equant	80	10	5	5	0	Grt lhz	G9	90.89	91.96	91.17	81.22	Cpx lobate to indented. Ol heavily serp	Yes	Yes	No
483806d1	Coarse equant to weak porphyroclastic	87	5	3	5	0	Grt lhz	G9	90.95	92.02	90.97	82.53	Cpx lobate to indented. Ol heavily serp	Yes	Yes	No
491719	Mosaic porphyroclastic	68	20	5	7	0	Grt lhz	G9	91.12	92.13	92.03	83.21	Cpx has subhedral shape. Porphyroblasts are deformed.	Yes	Yes	No
491731	Mosaic porphyroclastic	75	5	5	15	0	Grt lhz	G9	91.69	92.62	91.96	85.45	Cpx has turbid alteration rims. Deformed porphyroblasts.	Yes	Yes	No
474521	Coarse tabular to porphyroclastic	85	10	0	0	5	Sp-hzb	n.a.	91.72	91.28	n.a.	n.a.	Extensively serpentinized	No	Yes	Yes
474544	Coarse tabular	95	0	0	0	5	Sp dun	n.a.	92.74	n.a.	n.a.	n.a.	Extensively serpentinized	No	Yes	Yes
474545	Coarse tabular	85	10	0	5	0	Grt hzb	G10	92.74	93.56	n.a.	83.42	Serpentinized and infiltrated by kimberlite	Yes	Yes	Yes
474557	Porphyroclastic	85	0	15	0	0	Weh	n.a.	n.a.	n.a.	n.a.	n.a.	Heavy serpentinized and carbonate infiltrated.	No	No	Yes
474566	Coarse equant	75	10	0	15	0	Grt hzb	G10	92.64	93.49	n.a.	83.23	Strongly serpentinized ol	Yes	Yes	Yes
477404	Porphyroclastic	>85	0	<5	5	0	Weh	G9	89.76	0.00	91.31	80.05	Kink banded and weakly serp ol. Carbonate infiltrated.	Yes	Yes	No
477406c2	Coarse equant	>75	0	15	<5	0	Weh	G12	92.48	0.00	93.46	82.08	Carbonate infiltrated.	Yes	Yes	No
477419	Porphyroclastic	>80	0	<5	<5	0	Weh	G5	89.09	0.00	90.34	79.91	Carbonate infiltrated.	Yes	Yes	No
481814b	Porphyroclastic	>69	0	10	15	1	Weh	G9	88.49	0.00	89.94	78.03	Kink banded and weakly serp ol. Carbonate infiltrated.	Yes	Yes	No

Table 2 (*continued*)

Sample	Texture	Ol%	Opx%	Cpx%	Grt%	Spl%	Rock type	Grt type	Ol Mg#	Opx Mg#	Cpx Mg#	Grt Mg#	Remarks	*P–T* subset	Online table B	Wittig et al., 2008
488836	Coarse equant_very serpentinized	85	0	0	0	5	Sp dun	n.a.	91.03	n.a.	n.a.	n.a.	Extensively serpentinized	No	Yes	Yes
488850	Coarse tabular	>90	0	0	0	5	Sp dun	n.a.	93.11	n.a.	n.a.	n.a.	Extensively serpentinized	No	Yes	Yes
488858	Coarse equant	85	5	0	0	5	Sp dun	n.a.	n.a.	88.07	n.a.	n.a.	Extensively serpentinized	No	Yes	Yes
488866	Granublastic	75	5	0	0	10	Sp dun	n.a.	86.14	86.35	n.a.	n.a.	Carbonate infiltrated.	No	Yes	Yes
488869	Serpentinized	95	0	0	0	5	Sp dun	n.a.	87.66	n.a.	89.55	n.a.	Extensively serpentinized	No	Yes	Yes
488882	Porphyroclastic	60	20	0	0	>1	Hzb	n.a.	n.a.	n.a.	n.a.	n.a.	Extensively serpentinized	No	No	Yes
488883	Coarse tabular	98	0	0	0	2	Sp dun	n.a.	93.01	n.a.	n.a.	n.a.	Serpentinized	No	Yes	Yes
488888	Coarse serpentinized	95	0	0	0	5	Sp dun	n.a.	91.03	n.a.	n.a.	n.a.	Extensively serpentinized	No	Yes	Yes
488890	Coarse to weak porphyroblastic	98	0	0	0	2	Sp dun	n.a.	89.14	n.a.	n.a.	79.02	Extensively serpentinized	No	Yes	Yes
488892	Coarse	94	0	0	3	3	Sp-grt dun	G12	90.47	n.a.	90.97	86.15	Extensively serpentinized	Discarded	Yes	Yes
490301	Coarse equant	75	10	0	15	0	Grt hzb	G10	93.45	94.19	n.a.	84.60	Extensively serpentinized	Yes	Yes	No
491810a2	Porphyroblastic.	90	0	0	10	0	Grt dun	G1	92.74	n.a.	n.a.	n.a.	Extensively serpentinized	No	Yes	No
Mh24.05b1	Coarse tabular	75	15	0	10	0	Grt-sp hzb	G10D	92.51	93.60	n.a.	83.44	Serpentinized and some carbonate infiltration.	Discarded	Yes	No
Mh25.05a2	Coarse tabular	79	15	5	5	1	Grt-sp lhz	G9	92.33	93.20	95.25	79.61	Cpx has turbid alteration rims. Grt are elongate.	Yes	Yes	No

References to other tables and additional work.
Discarded: not equilibrated sample, data not included here.

richterite or ilmenite (e.g. Gurney and Harte, 1980). Three of the 27 samples displayed severe discrepancies between pressures and temperatures calculated using several *P–T* formulations and were consequently discarded from the study. The results for 24 peridotite xenoliths considered to be close to equilibrium are presented below.

4.1. Petrography

The mantle xenoliths investigated in this study are typically 2–15 cm across, have coarse grained textures and variable modal contents of especially garnet and pyroxene (Table 2). Most of the investigated samples show some secondary alteration, typically expressed as serpentinisation (Fig. 2C), pyroxene alteration (Fig. 2C and D) kelyphitic rims on garnet, and introduction of melt from the host rock.

Eleven of the 17 investigated garnet lherzolite samples display coarse textures (e.g. Fig. 2A), two are porphyroclastic, two are porphyroclastic mosaic (Fig. 2B) and one sample is granoblastic. The samples are texturally equilibrated with respect to olivine, garnet and orthopyroxene. Due to an apparent secondary alteration of the clinopyroxene the textural and chemical systematics of this mineral are less clear. The clinopyroxenes typically display lobate shapes with turbid alteration rims (e.g. Fig. 2D) that possess a heterogeneous element distribution. The crystal interior, however, has a homogeneous element distribution. Several orthopyroxene grain rims are also altered and display thin, clinopyroxene-like films on grain boundaries.

Four garnet harzburgites are included in this study, one with porphyroclastic texture and three with coarse textures. Olivine suffers from extensive serpentinisation and several fresh orthopyroxene grains appear disrupted at depth. A few of the orthopyroxene grains have thin films on grain boundaries resembling clinopyroxene.

Four garnet wehrlite xenoliths from the Maniitsoq area are included in this study. A gradual transformation is seen within these samples from coarse to porphyroclastic textures. All the samples show secondary metasomatism. Most clinopyroxene grains are 1–3 mm in diameter and have turbid to anhedral shapes and a spongy alteration rim. They appear kink-banded and rims contain numerous fluid inclusions, phlogopite and disseminated opaque phases. Some carbonate infiltration is also evident.

Based on petrographic examination it is reasonable to consider that the cores of the minerals represent ambient mantle conditions and can be used to estimate *P–T* conditions. Textural equilibration between olivine, orthopyroxene and garnet appears convincing for most samples, but equilibration of clinopyroxene is more suspect due to their predominantly lobate crystal form.

4.2. Mineral compositions

Mineral compositions for all analysed phases in the SW Greenland peridotite xenoliths are given in Supplementary Table B. The compositions are broadly similar to those of peridotites from the Slave craton (Pearson et al., 1999; Kopylova et al., 1999) and the Kaapvaal craton (e.g. Finnerty and Boyd, 1984; Simon et al., 2003), though include some key differences. Orthopyroxenes within the Greenlandic peridotite suite have slightly lower MgO and SiO_2 concentrations than those in Slave and Kaapvaal craton peridotites (Fig. 3A). TiO_2 contents of Greenlandic peridotite minerals are often greater than in other cratons and this is most obvious for a group of garnets (Fig. 3B). Olivines from the SW Greenlandic sample suite show Mg-numbers (Mg#;100*Mg/[Mg + Fe)]) between 88 and 94, with the majority of samples falling between 91 and 93. Similar values are observed in peridotites from the Slave and Kapvaal cratons and such olivine compositions are typical of cratonic peridotites in general (Bernstein et al., 2007; Pearson and Wittig, 2008).

The peridotite mineral compositions selected for *P–T* work show little variation between samples from the Kangerlussuaq, Sarfartoq and Maniitsoq areas. Orthopyroxene from porphyroclastic samples is generally more FeO rich than coarse-textured orthopyroxene. The lherzolites show a broad range in chemical composition for all minerals, and have Mg# for olivine between 88.3 and 92.7. Orthopyroxene in

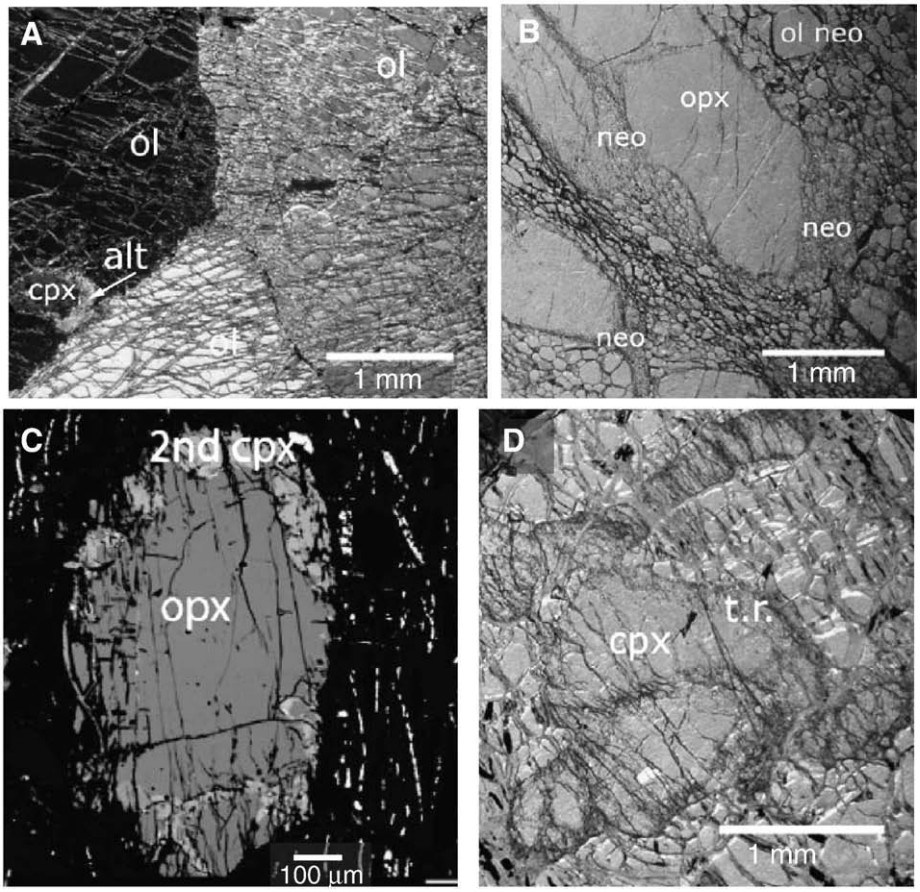

Fig. 2. Representative photomicrographs. A) CPL. Coarse textured lherzolite (477406) where veins of serpentine cut the olivine (ol) grains and the grain boundaries appear slightly irregular. Note the incipient carbonate pseudomorphism/alteration (alt) of the cpx. B) CPL. Garnet lherzolite (491431). Orthopyroxene showing neoblast formation (neo) in a mosaic-porphyroclastic textured lherzolite. C) BSE image of garnet lherzolite (464637). Orthopyroxene with an alteration rim of secondary (2nd) cpx. Very fine-grained phlogopite, spinel (sp) and chlorite (chl) is also present, however cannot be recognized on this BSE image. The matrix (dark background with white stringers) is serpentinized olivine. D). PPL of garnet lherzolite (483806). Lobate vermicular clinopyroxene with turbid alteration rim (t.r.).

harzburgites is low in CaO, Al_2O_3, TiO_2 and Na_2O, while both olivine and orthopyroxene in harzburgites consistently show higher Mg# (e.g. Ol Mg# of 91.3–93.5) than in lherzolites, a feature that Gurney et al. (1979) ascribe to equilibrated parageneses (not shown). The harzburgitic garnets are low in CaO (G10) and span a wide range in Cr_2O_3 content (~3–10 wt.%). Wehrlitic minerals span a wide compositional range,

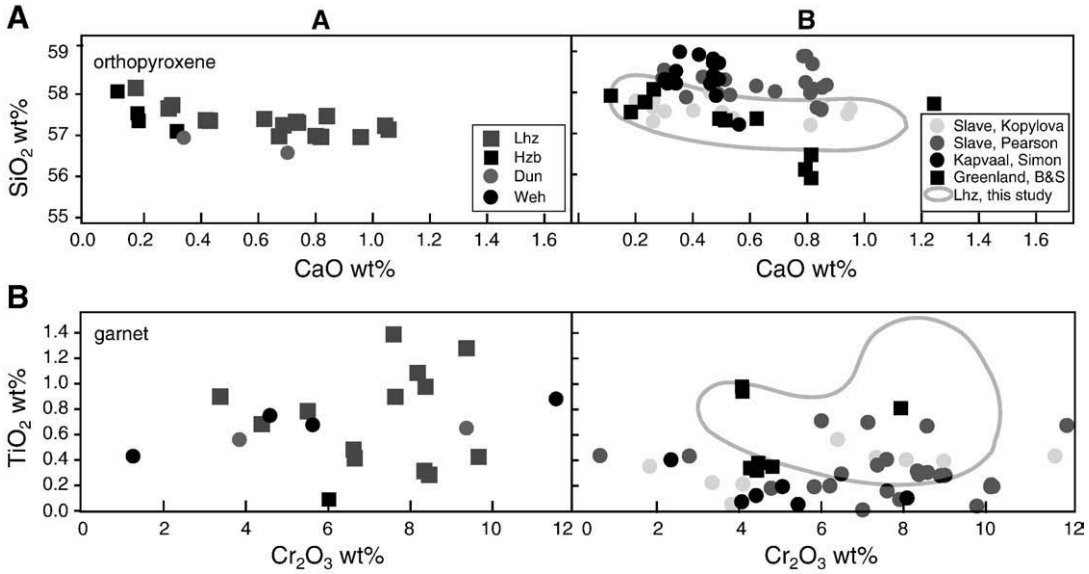

Fig. 3. Chemical variations of orthopyroxene (A) and garnet (B) illustrating a few keypoints. Column A represents data from this work only. Column B compares the lherzolites from this work with data from the Slave (Kopylova et al., 1999 and Pearson et al., 1999) and the Kaapvaal (Simon et al., 2003) cratons. Additional data from Greenland by Bizzarro and Stevenson (2003) is also given. A) orthopyroxene: CaO vs. SiO2 content (wt.%) illustrating that the Greenlandic orthopyroxene overlaps with a low-SiO_2 range from Kaapvaal and Slave peridotites. B) Garnet: Cr_2O_3 vs. TiO_2 illustrating the trend to higher TiO_2 contents for the Greenlandic suite compared to the other cratons.

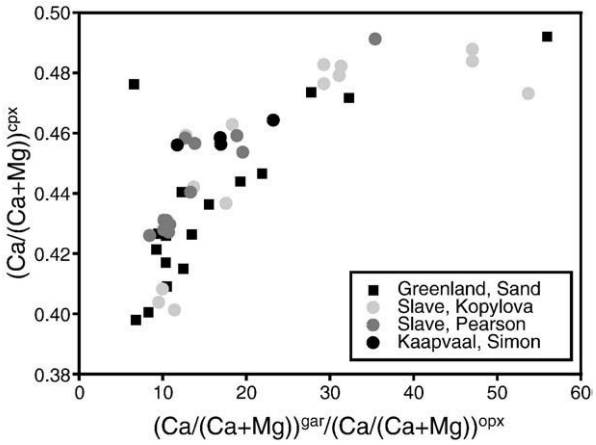

Fig. 4. Variation in the mineral ratios: $(Ca/(Ca+Mg))^{gar}/(Ca/(Ca+Mg))^{opx}$ vs. $(Ca/(Ca+Mg))^{cpx}$. The Greenlandic samples correspond in general to the trend defined by data for lherzolite xenoliths from the Slave, Kaapvaal cratons (references as in Fig. 3).

overlapping the lherzolitic samples, with garnet plotting in the G5, G9 and G12 fields of Grütter et al. (2004) and Schulze (2003).

As mentioned previously, textural evidence for clinopyroxene equilibration is questionable though our work does not include trace element or isotopic data that would definitively support metasomatic introduction of late clinopyroxene (e.g. Pearson and Nowell, 2002; Simon et al., 2003). It is therefore important to carefully scrutinize major element data to establish chemical equilibrium in samples used for *P–T* determinations. Chemical equilibrium between garnet, orthopyroxene and clinopyroxene is assessed according to the correlated ratio $(Ca/(Ca+Mg))^{grt}/(Ca/(Ca+Mg))^{opx}$ vs. $(Ca/(Ca+Mg))^{cpx}$ (after Finnerty and Boyd, 1984). The correlated ratio for the Greenlandic peridotite suite overlaps that of xenoliths from northern Lesotho, South Africa (Finnerty and Boyd, 1984), and the Slave and Kapvaal cratons (Fig. 4) (The former is not shown.) and is considered strong evidence in favor of chemical equilibration of clinopyroxenes with garnet and orthopyroxene. Also, garnet compositions indicate equilibration with clinopyroxene (i.e., there are no subcalcic "G10" garnets in any of the clinopyroxene-bearing rocks).

4.3. Geothermobarometry

Comparison and evaluation of results obtained from different *P–T* combinations are complicated by a range of factors, such as calibration shortcomings, extrapolation of *P–T* formulations to pressure, temperature and compositional ranges outside experimental conditions, analytical errors and lack of mineral equilibration. Determination of thermobarometer combination(s) most suitable to a particular xenolith suite is therefore not straightforward (e.g. Harley, 1984). Thermobarometry based on element exchange reactions between two minerals are believed to be more reliable than some single-mineral methods (Smith, 1999), and in addition element exchange reactions between two minerals provide better evaluation of *P–T* results. We take the opportunity of comparing xenolith-based thermobarometry results with single-mineral methods because the latter are of particular interest to exploration geologists. Moreover, Grütter (2001) argued that the well calibrated single-clinopyroxene thermometer of Nimis and Taylor (2000) yields reliable temperature estimates when compared to Fe–Mg exchange reactions between two minerals; this is also the case for TNT in combination with aluminum in orthopyroxene barometry.

4.4. P–T results

Results obtained for PMC and PBKN barometry in combination with four geothermometers (TBKN, TCa-in-opx, THarley and TO'Neill) for the SW Greenland lherzolites are listed in Supplementary Table C and illustrated in Fig. 5. Iteratively calculated *P–T* results for PMC and PBKN are displayed with different symbols, but on the same panels in Fig. 5, for ease of comparison. For simplicity, the PNG barometer formulation is not shown in Fig. 5 as it yields results for this suite that are very similar to PMC below 5.5 GPa. The lherzolites are generally derived from pressures of 3–7 GPa using PMC or 2.5–6 GPa using PBKN. The application of several different thermometers produces a

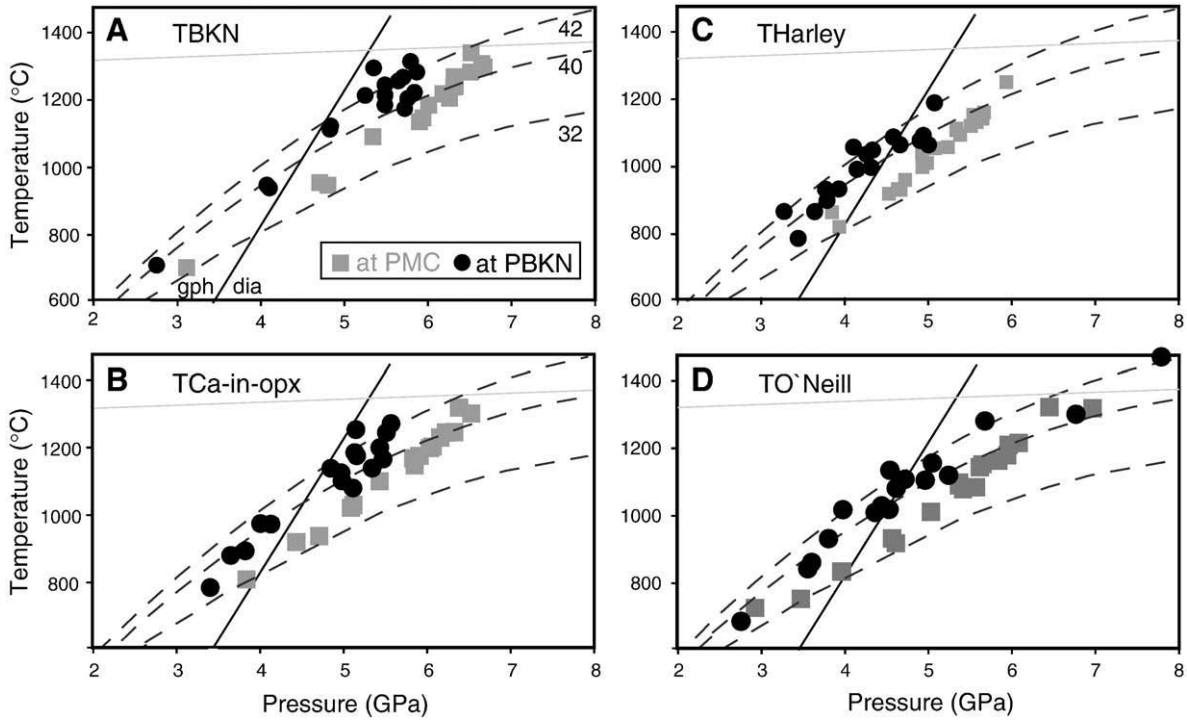

Fig. 5. Xenolith-based geotherms for lherzolites of this study. The barometers used are PMC (grey squares) and PBKN (black circles). The thermometers used are TBKN (A), TCa-in-opx (B), THarley (C), and TO'Neill (D). Geotherms in mW/m^2 (dashed lines) are from Pollack and Chapman (1977), and the diamond–graphite equilibrium is from Kennedy and Kennedy (1976). The mantle adiabat (grey line) corresponds to a potential temperature of 1300 °C and a 0.5 °C/km geothermal gradient (after Rudnick and Nyblade, 1999).

broadly similar temperature range irrespective of the choice of barometer. However, certain features of the *P–T* trends are dependent on the thermobarometer pair used, as observed in Fig. 5.

The apparent xenolith geotherms calculated using PMC (Fig. 5, grey squares) display linear trends that transect the curved model-conductive geotherms of Pollack and Chapman (1977). At low-*T* the data points broadly follow a ~33 mW/m^2 gradient at pressures up to ~5 GPa, where they deviate from the 33 mW/m^2 model and transect 32–41 mW/m^2 model geotherms. *P–T* estimates calculated using PBKN (Fig. 5 black circles) scatter between the 40 and 42 mW/m^2 geotherms and are semi-confined by the curvature of the geotherms. Generally, the two-pyroxene thermometers (TBKN and TCa-in-opx) show increased scatter towards higher temperatures and pressures. Furthermore, the two-pyroxene thermometers produce a cluster as opposed to the more linear distribution observed for the Fe–Mg exchange thermometers (THarley and TO'Neill). The depression observed in temperature for the Fe–Mg exchange thermometers is expected, as the Fe–Mg based temperatures are considered to be minima due to the assumption that $Fe^{2+} = Fe^{total}$ (Harley, 1984; O`Neill and Wood, 1979). These trends are similar for combinations with the PMC, PBKN or PNG barometers. We thus conclude that the majority of the mutual variation of data points seen in Fig. 5 is a function of the thermometer formulation applied, and is not an artifact of error propagation from the pressure formulation. However, the choice of barometer has considerable effect on the *P–T* results for the sample suite relative to the diamond–graphite stability field. An extreme example of this effect is for iterations with THarley (Fig. 5C) where 18 of 20 samples are in the diamond stability field using the PMC formulation in contrast to only five samples being in the diamond stability field using the PBKN formulation.

5. Discussion

5.1. Barometry

To address the disagreement between the Al-in-opx barometers in more detail, several comparisons were made. Calculation of pressure using an iterative approach produces linear but different correlations between the three barometers: PBKN, PMC and PNG (not shown). Pressures produced by the PBKN formulation are lower than PMC and PNG by ~1 ± 0.5 (2σ) GPa. Applying a preset temperature of 1100 °C to the barometers, the calculated scatter in pressure is pronounced, as illustrated in Fig. 6 (A, B). The results obtained using the PMC and PNG formulations show good agreement, to within 0.1 ± 0.3 (2σ) GPa (Fig. 6C). Pressures estimated with PBKN, PMC and PNG were compared with the Cr-in-cpx barometer PNT which is based on a different exchange reaction and as such yields an independent test of the Al-in-opx barometers. PNT barometry results are consistent with the higher pressures found using PMC and PNG, the former with a mean difference of 0.2 ± 0.6 GPa (2σ) (Fig. 6D). The agreement between these different formulations, including one based on a different exchange reaction, indicates that pressures derived using the PBKN formulation for this suite of peridotites may not be as reliable as pressures obtained with PMC, PNG or PNT.

5.2. Thermometry

Further detailed evaluation of pyroxene-solvus and Fe–Mg exchange thermometers gives the following results for the Greenlandic sample suite (Figs. 5 and 7): a) thermometers based on the same exchange reaction (the 2-pyroxene and the Fe–Mg thermometers) yield mutually consistent results. b) Comparisons with TBKN only shows limited scatter when compared to TCa-in-opx. c) TCa-in-opx compared with THarley and TO'Neill show good mutual correlations. d) At higher temperatures, THarley underestimates the temperature compared to TBKN and TO'Neill. e) The TBKN formulation typically yields 60–80 °C higher

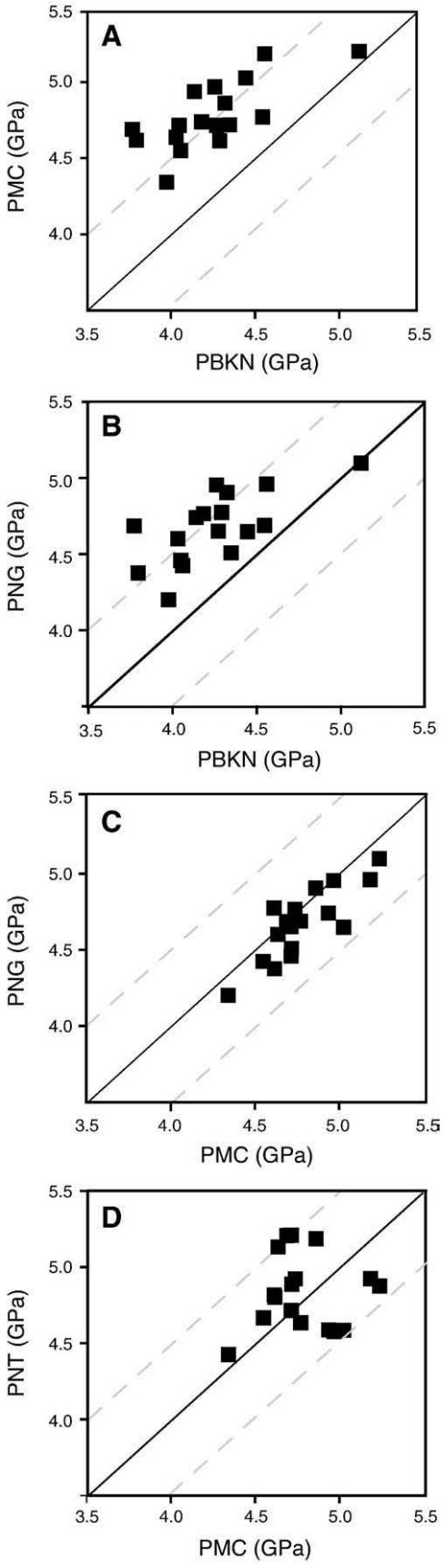

Fig. 6. Barometric results calculated at a preset temperature of 1100 °C. The grey lines represent 0.5 GPa deviations from the black 1:1 line. A) PBKN vs. PMC where PMC is observed to yield higher pressures than PBKN. B) PBKN vs. PNG where PNG is observed to yield higher pressures than PBKN. C) PMC vs. PNG showing comparability along the 1:1 line. D) PMC vs. PNT is comparable along the 1:1 line with increasing scatter at higher pressure.

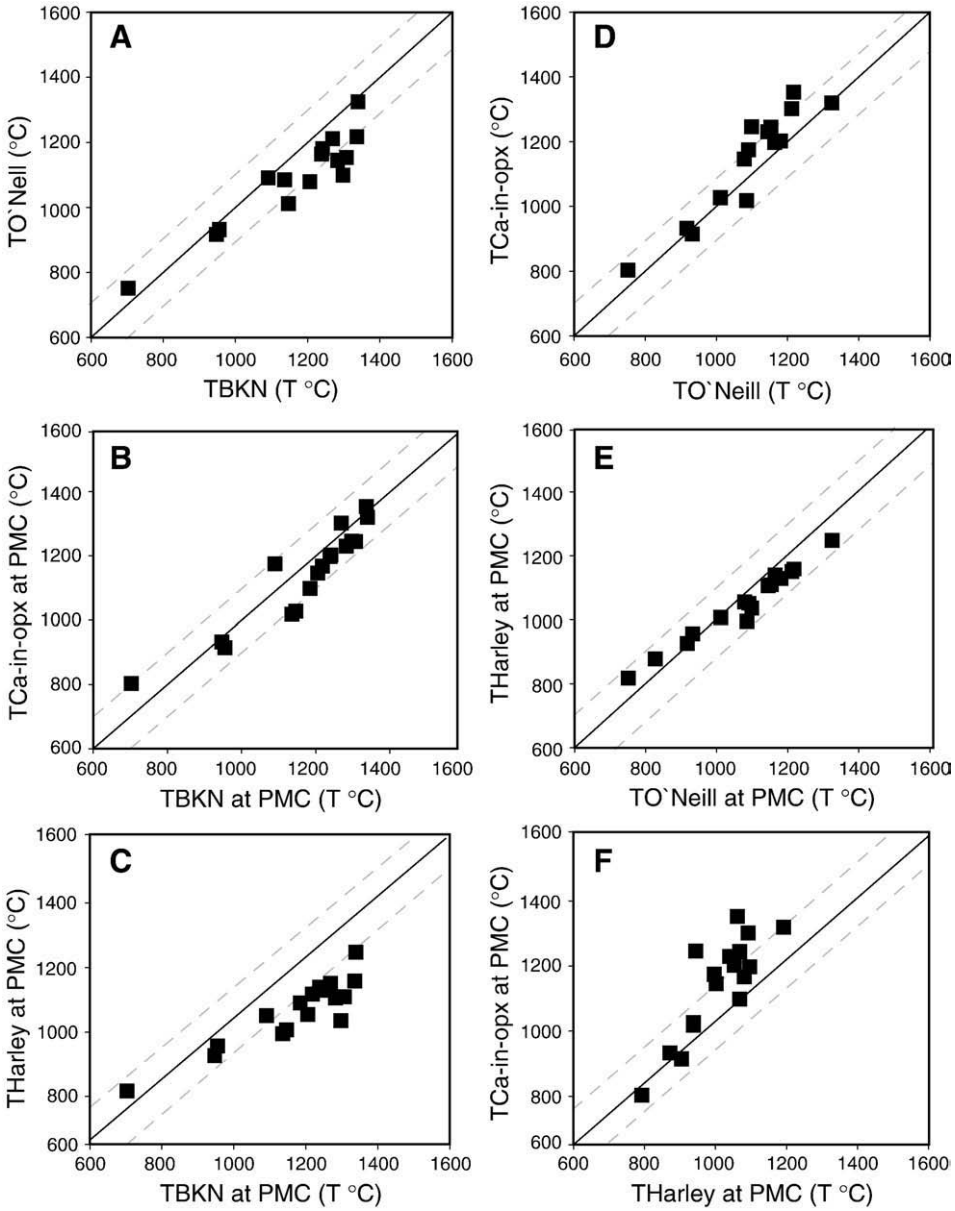

Fig. 7. Comparisons of the thermometer formulations calculated by means of iteration with PMC. The grey dashed line represents a 100 °C deviation from the black 1:1 line. A) TBKN vs. TO'Neill, where TBKN generally yields higher temperatures with ~100 °C. B) TBKN vs. TCa-in-opx showing near-consistent results, C) TBKN vs. THarley where TBKN produces considerable higher temperatures at high-T. D) TO'Neill vs. TCa-in-opx show good correlation, however, TCa-in-opx produces slightly higher temperatures at high-T. E) TO'Neill vs. THarley show good correlation, however, THarley produces consistently higher temperatures at low-*T* and lower temperatures at high-T than TO`Neill. F) THarley vs. TCa-in-opx shows correlation at low-*T*, however at high-T the TCa-in-opx produces considerably higher temperatures than THarley.

temperatures than the other thermometers (see also Grütter and Moore, 2003). Since results from the TCa-in-opx, TO`Neill, and THarley formulations correlate reasonably well, and differ from TBKN, the latter is potentially inapplicable to this data set (see Sand, 2007 for more detail) and is not used further. In summary, we conclude that the various distributions in *P–T* space between thermobarometers are a function of the thermometer formulation used, and not an artifact of error propagation from the calculation of equilibration pressures.

5.3. Assessment of mineral equilibration and favored P–T combination

The closely comparable results produced by TCa-in-opx, TO'Neill and THarley support the petrographic and chemical indications of mineral equilibrium between orthopyroxene, garnet and olivine. The fair correlation between TBKN and TCa-in-opx suggests mutually equilibrated clinopyroxene and orthopyroxene, however, as the TBKN thermometer is considered inapplicable to this sample suite, we substitute TNT as the cpx–solvus thermometer of interest, in part following similar suggestions made earlier (Grütter, 2001; Grütter and Moore, 2003). A good agreement in calculated temperatures is observed when comparing results obtained using the TNT and TCa-in-opx (at PNG) (Fig. 8A). This supports the chemical evidence of equilibrated clinopyroxene, despite petrographic evidence suggesting otherwise. Comparison of the resulting pressures from PNT–TNT with PNG–TNT (Fig. 8B) shows an agreement between the two pressure formulations of 0.5 GPa. It is emphasized that the PNT–TNT combination appears suitable to this xenolith suite, providing support for its role as an important tool for the exploration industry. The TNT formulation is here favored over the TCa-in-opx thermometer for clinopyroxene-bearing assemblages, as the former contains TiO_2 in the formulation and the SW Greenland

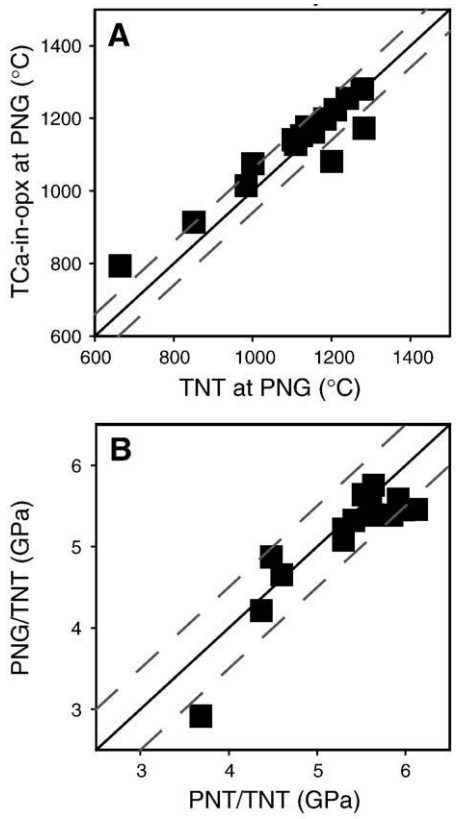

Fig. 8. A) TNT vs. TCa-in-opx, both calculated iteratively with PNG. Most estimates are within an error of 60 °C (dashed lines). B) Comparability of the geobarometers PNT and PNG, both calculated iteratively with TNT. Most estimates are within an error of ±0.5 GPa (grey dashed line) The solid black line represents a 1:1 line.

peridotites appear to be anomalous in their mineral TiO_2 contents. Because the TO'Neill formulation appears to expand the distribution of samples in *P–T* space this formulation is only applied to harzburgites.

5.4. P–T distribution

In order to include more samples in the *P–T* array for the SW Greenland region, the mineral dataset from Bizzarro and Stevenson (2003) has been recalculated using our favored thermobarometer combinations. *P–T* estimates for lherzolites are calculated using PNT–TNT and for harzburgites the combination PNG-TO'Neill is used. We extrapolated wehrlites to the geotherm by calculating TNT at a preset *P* (4.5 or 5 GPa) and note this approach formally yields minimum temperature estimates, given the absence of orthopyroxene. The resulting xenolith-based geotherm (Fig. 9A) consists of 32 *P–T* estimates and shows a *P–T* distribution from 2.8 GPa and 660 °C to 6.4 GPa and 1340 °C. At temperatures below 1000 °C the equilibrium conditions fall within the 32–40 mW/m^2 model-conductive geotherms of Pollack and Chapman (1977). At temperatures above ~1000 °C the equilibrium conditions transect the geotherms, scattering between the 40 and 42 mW/m^2 geotherms. However, the model geotherms of Pollack and Chapman (1977) have been shown to yield an erroneously hot gradient below 120 km, resulting in unrealistic curvature at depth (Rudnick and Nyblade, 1999). Most samples from this study follow a simpler steady-state geotherm (e.g. McKenzie et al., 2005) with an approximated model heatflow of 38 ± 2 mW/m^2 (not shown).

5.5. Thickness of the SCLM

The minimum thickness of the SCLM is here given by the deepest xenolith. The deepest xenolith on Fig. 9 is a harzburgite (G9 garnet) from Bizzarro and Stevenson (2003) and yields a thickness of 215 km. The deepest xenolith from the new data presented here is a lherzolite and gives an estimate of the minimum thickness of the SCLM of 190 km. The intersection between the xenolith-geotherm and the mantle adiabat, gives an estimate of the maximum thickness of the thermal boundary layer as defined by Eaton et al. (2009) which we take to approximate the base of the lithosphere. The adiabat used here corresponds to a 1300 °C potential temperature and a 0.5 °C/km gradient (Rudnick and Nyblade, 1999), applying a first order regression ($r^2 = 0.955$, excl. wehrlites) the base of the lithosphere in this study is estimated to be at a maximum of 215 km (Fig. 9A). Sampling of equilibrated xenoliths by the host magma appears to have been more efficient in the deeper parts of the SCLM whereas shallower samples are more scarce. Four of the highest *P–T* samples have porphyroclastic or mosaic textures and could be affected by melt percolation and heat advection (e.g. Smith, 1999). Excluding these samples from the regression yields a similar maximum thickness of the SCLM of 220 km. These estimates are in good agreement with the typical maximum depths of Archean lithosphere estimated by seismology (e.g. McKenzie and Priestley, 2008 and Eaton et al., 2009).

These findings compare well with the study of Garrit et al. (1996), except that no lateral variation in geothermal gradient is observed here and we emphasize the abundance of much depleted lithologies such as dunites and harzburgites. The recalculated *P–T* results of Bizzarro and Stevenson (2003) plot along a hotter geotherm than originally proposed as a result of the application of the PBKN formulation by these authors. Grütter and Moore (2003) applied the PNG–TNT combination to a comprehensive data set of Canadian and South African garnet lherzolite xenoliths and established that the Canadian xenolith *P–T* data define distinctly separate geothermal arrays for Somerset Island, Kirkland Lake and the Slave craton. In our study it appears that the Greenlandic suite correlates well with the low-*T* range of Kirkland Lake and the high-*T* range from the Slave craton. The Greenlandic xenolith suite appears to define a cooler geotherm than peridotite xenoliths from Gibeon (Boyd et al., 2004), Northern Lesotho and Kimberley mines (Southern Africa; Finnerty and Boyd, 1984). This trend is supported by recent investigations in the Sarfartoq area by Grütter and Tuer (2009-this volume).

5.6. Mantle stratigraphy

Detailed examination of the xenolith-derived geotherm from SW Greenland reveals two groups of data in *P–T* space (Fig. 9A): a low-*T*

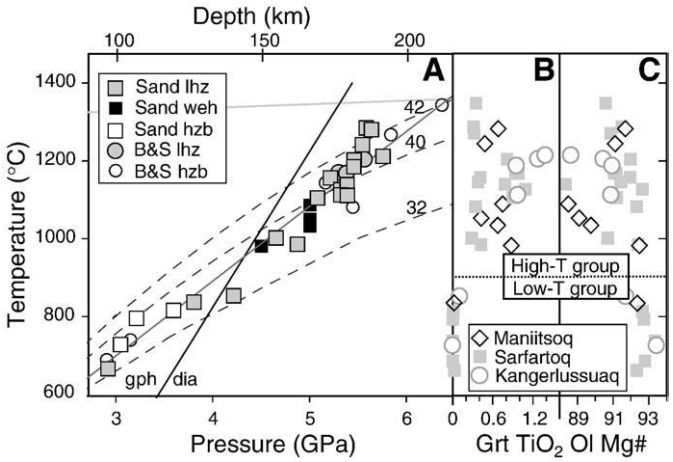

Fig. 9. A) Pressure and depth vs. temperature distribution of the xenolith-based geotherm of this study (squares), supplemented with recalculated data from Bizzarro and Stevenson (2003) (circles). The majority of the lherzolites (lhz) come from greater depths than the harzburgites (hzb). Conversion of pressures to depth: 1 GPa = 33.3 km. Geotherms and adiabat as in Fig. 6. Grey dashed line represents linear regression for calculation of the maximum thickness of the thermal boundary layer. B) TiO_2 in garnets in wt.% vs. temperature (TNT at PNG). C) Olivine Mg# vs. temperature (TNT at PNG). Different symbols in B) and C) reflect three study areas (see legend). No distinctions between the three areas are evident.

group separated from a high-*T* group by a circa 30 km gap between 810 °C and 980 °C where only one investigated sample is located. The wehrlites appear to correlate with the high-*T* group since their minimum temperatures appear restricted to the lower end of the high-*T* group. Lherzolites are present across the full high-*T* range. Equilibrated harzburgites appear to be restricted to relatively shallow levels and none are observed in the high-*T* suite, with the exception of four harzburgites from the study of Bizzarro and Stevenson (2003). Three of the four harzburgites contain garnets that plot in lherzolite field of Grütter et al. (2004) (G9) indicating equilibration with clinopyroxene or late stage clinopyroxene metasomatism. Additional information on lithological and compositional variations with depth is revealed by considering the TiO_2 contents in garnet (Fig. 9B) and olivine Mg# (Fig. 9C). A clear distinction is observed in TiO_2 values of the garnets between the low-*T* and high-*T* group, with all samples in the high-*T* group having TiO_2 values exceeding 0.25 wt.% (Fig. 8B). TiO_2 contents in the low-*T* group are below 0.15 wt.%. The ranges for olivine Mg# generally show a decrease with depth where the low-*T* group ranges between 92 and 93 and the high-*T* group spans compositions from 88 to 93. A textural variation with depth is also observed in the SW Greenlandic sample suite, with coarse textures only observed for low *P*–*T* samples. In contrast, both coarse and porphyroclastic to mosaic textures are present in the high-*T* group with only mosaic-porphyroclastic at $T>1200$ °C. These observations indicate a layered mantle for equilibrated xenoliths beneath SW Greenland, with a relatively shallow depleted section dominated by harzburgite and subordinate lherzolite from ~90 to 115 km and a more compositionally heterogeneous mantle section comprising harzburgite, lherzolite and wehrlite from 140 to 215 km (Fig. 9B–C). It should be noted that the sampling strategy with a focus on equilibrated lherzolites for *P*–*T* estimates potentially has biased this image of the mantle. However, these findings correspond with the increasing fertility to depth reported in previous studies (Bizzarro and Stevenson, 2003; Garrit et al., 1996; Griffin et al., 2004).

5.7. Diamond potential

As noted above, the xenolith suite was collected across a tectonic suture separating two crustal domains with distinct histories and compositions, and their depth extent into the underlying mantle is potentially constrainable with our xenolith data set. From the present dataset it is not possible to discern significant variations of the mantle geotherm across the Kangerlussuaq, Sarfartoq and Maniitsoq geological domains. The ~1.8–1.9 Ga Nagssugtoqidian orogeny does not appear to have had any residual influence on the *P*–*T* gradients nor thickness of the SCLM at the time of sampling. Twenty-five of 32 analysed xenoliths were sampled from deeper than the intersection of the graphite–diamond transition (Kennedy and Kennedy, 1976) with the calculated geotherm (Fig. 9), with most samples from Maniitsoq falling within the diamond stability field. These results indicate that a large proportion of the xenolith cargo of a given host volcanic rock could be derived from within the diamond stability field. The observations are consistent with the discovery of diamonds in the region by several exploration companies.

The geometry of the estimated geotherm, extrapolated to a mantle adiabat implies that 75 km of the SCLM occurs within the diamond stability field. When viewed solely from thermal considerations and the depth of the lithosphere at ca. 600 Ma, the SW Greenlandic SCLM, including the portion north of the Proterozoic deformation front, possesses excellent diamond potential. Preliminary results of Re–Os dating also indicate that the age of peridotitic lithosphere across this region, and specifically across the Proterozoic deformation front, is consistently Archean (Webb, 2007; Pearson and Wittig, 2008; Wittig et al., 2008). Hence, it appears that the entire region of our sampling was underlain by thick, diamond-facies Archean lithospheric mantle at ca. 600 Ma. Thus, based on the data presented here the diamond exploration should be targeted in the area north of the deformation front, as well as into the undeformed craton interior to the south. Detailed seismological studies are required to evaluate the depth of lithosphere that still remains beneath this part of the North Atlantic Craton following Tertiary rifting and magmatism.

6. Conclusions

A detailed thermobarometry study has been carried out on a new suite of peridotite xenoliths from SW Greenland. On the basis of extensive testing and evaluation, the preferred thermobarometer combination for this sample suite is PNG–TNT for garnet-lherzolites and PNG–TO'Neill for garnet harzburgites. The resulting calculated xenolith-based geotherm can be divided into low-*T* (660–850 °C) and high-*T* (980 °C–1340 °C) segments and yields a maximum SCLM thickness of 215–220 km depth at ca. 600 Ma ago. This result is in good agreement with the typical depths of Archean lithosphere estimated by seismology (e.g. McKenzie and Priestley, 2008). The xenoliths fall along a geotherm similar to peridotites from the Slave and Superior (Kirkland Lake) cratons, but cooler than geotherms typically recorded by xenolith suites from Southern Africa. No apparent variation in geothermal gradient can be discerned between the three study areas in SW Greenland at the time of kimberlitic magmatism and therefore no thermal effects of a major orogeny ~2 Ga ago are recorded in the available *P*–*T* estimates. Our findings indicate a layered mantle for equilibrated xenoliths beneath SW Greenland with an increase in fertility with depth.

The SW Greenland region possesses an excellent diamond potential because 75 km of the sampled SCLM was within the diamond stability field at the time of sampling by magmatism and 25 of 32 analysed xenoliths were sampled from the diamond stability field.

Acknowledgements

We would like to thank Berit Wenzel and Hanne Lamberts for technical and practical help and discussions. Hudson Resources Inc. is acknowledged for provision of Silly Kimberlite samples. Also, Norman Pearson is thanked for supplying chemical data from the Slave Craton. Agnete Steenfelt, Karsten Secher and Lotte Melchior are thanked for scientific discussions. Stefan Bernstein and Jacqueline Malarkey are thanked for constructive reviews and Herman Grütter is thanked for editorial assistance.

Appendix A. Supplementary data

Supplementary data associated with this article can be found, in the online version, at doi:10.1016/j.lithos.2009.05.012.

References

Bernstein, S., Kelemen, P., Brooks, C.K., 1998. Depleted spinel harzburgite xenoliths in Tertiary dykes from East Greenland: restites from high degree melting. Earth and Planetary Science Letters 154, 221–235.

Bernstein, S., Kelemen, P.B., Hanghøj, K., 2007. Consistent olivine Mg# in cratonic mantle reflects Archean mantle melting to the exhaustion of orthopyroxene. Geology 35, 459–462.

Bizzarro, M., Stevenson, R.K., 2003. Major element composition of the lithospheric mantle under the North Atlantic craton: evidence from peridotite xenoliths of the Sarfartoq area, southwestern Greenland. Contributions to Mineralogy and Petrology 146, 223–240.

Boyd, F.R., Pearson, D.G., Hoal, K.O., Hoal, B.G., Nixon, P.H., Kingston, M.J., Mertzman, S.A., 2004. Garnet lherzolites from Louwrencia, Namibia: bulk composition and P/T relations. Lithos 77, 573–592.

Brey, G.P., Köhler, T., 1990. Geothermobarometry in 4-phase lherzolites.2. New thermobarometers, and practical assessment of existing thermobarometers. Journal of Petrology 31, 1353–1378.

Canil, D., O'Neill, H.S.C., 1996. Distribution of ferric iron in some upper mantle assemblages. Journal of Petrology 37, 609–635.

Eaton, D.W., Darbyshire, F., Evans, R.L., Grütter, H., Jones, A.G., Yuan, X., 2009. The elusive lithosphere–asthenosphere boundary (LAB) beneath cratons. Lithos 109, 1–22.

Finnerty, A.A., Boyd, F.R., 1984. Evaluation of thermobarometers for garnet peridotites. Geochimica Et Cosmochimica Acta 48, 15–27.

Finnerty, A.A., Boyd, F.R., 1987. Thermobarometry for garnet peridotites: basis for the determination of thermal and compositional structure of the upper mantle. In: Nixon, P.H. (Ed.), Mantle Xenoliths. Wiley, New York.

Garrit, D., 2000. The nature of Archaean and Proterozoic lithospheric mantle and lower crust in West Greenland illustrated by the geochemistry and petrography of xenoliths from kimberlites. Ph.D. Thesis, University of Copenhagen, Denmark,

Garrit, D., Griffin, W.L., O'Reilly, S.Y., 1996. Processes in Archaean and Proterozoic mantle in West Greenland. Journal of Conference Abstracts 1, 194.

Griffin, W.L., O'Reilly, S.Y., Doyle, B.J., Pearson, N.J., Coopersmith, H., Kivi, K., Malkovets, V., Pokhilenko, N., 2004. Lithosphere mapping beneath the North American plate. Lithos 77, 873–922.

Grütter, H.S., 2001. The thermobarometric basis for mantle stratigraphy and mantle mapping. Geophysical and Geochemical Imaging of Canada's upper mantle. KEGS (Canadian Exploration Geophysical Society) One-day Short Course for Diamond Explorationists, Toronto, March, 2001, pp. 1–12.

Grütter, H., Moore, R., 2003. Pyroxene Geotherms Revisited — An Empirical Approach Based on Canadian Xenoliths, Extended Abstracts, Eight International Kimberlite Conference, 272 (CD-ROM).

Grütter, H.S., Tuer, J., 2009-this volume. Modern single-grain thermobarometry techniques applied to mantle xenocrysts from the Sarfartoq area, Greenland. Lithos. doi:10.1016/j.lithos.2009.03.012

Grütter, H., Gurney, J.J., Menzies, A.H., Winter, F., 2004. An updated classification scheme for mantle-derived garnet, for use by diamond explorers. Lithos 77, 841–857.

Gurney, J.J., Harte, B., 1980. Chemical variations in upper mantle nodules from southern African kimberlites. Philosophical Transactions of the Royal Society of London. Series A, Mathematical and Physical Sciences 297, 273–293.

Gurney, J.J., Harris, J.W., Rickard, R.S., 1979. Silicate and oxide inclusions in diamonds from the Finsch kimberlite pipe. In: Boyd, F.R., Meyer, H.O.A. (Eds.), Kimberlites, Diatremes and Diamonds: their Geology and Petrology and Geochemistry. American Geophysical Union, Washington, DC.

Harley, S.L., 1984. An experimental study of the partitioning of Fe and Mg between garnet and orthopyroxene. Contribution to Mineralogy and Petrology 86, 359–373.

Harte, B., 1977. Rock nomenclature with particular relation to deformation and recrystallisation textures in olivine-bearing xenoliths. Journal of Geology 85, 279–288.

Hutchison, M.T., Frei, D., 2009, this issue. Kimberlite and related rocks from Garnet Lake, West Greenland, including their mantle constituents, diamond occurrence, age and provenance. Proceedings of the 9th International Kimberlite Conference. Lithos 112S, 318–333.

Hutchison, M.T., Heaman, L.M., 2008. Chemical and physical characteristics of diamond crystals from Garnet Lake, Sarfartoq, West Greenland: an association with carbonatitic magmatism. Canadian Mineralogist 46, 1063–1078.

Jensen, S.M., Lind, M., Rasmussen, T.M., Schjøth, F., Secher, K., 2003. Diamond exploration data from West Greenland. Danmarks og Grønlands Geologiske Undersøgelse Rapport, 2003/21, p. 50.

Jensen, S.M., Secher, K., Rasmussen, T.M., 2004. Diamond exploration data from West Greenland: 2004 update and revision. Danmarks og Grønlands Geologiske Undersøgelse Rapport, 2004/117, p. 90.

Jensen, S.M., Sand, K.K., Steenfelt, A., 2005. Regional distribution and chemistry of indicator minerals from in situ rocks and surficial deposits in the Maniitsoq and Sarfartoq regions. Extended abstracts vol, Workshop on Greenland´s diamond potential, 7–9 November 2005, Copenhagen. p 43.

Kalsbeek, F., 1976. Metamorphism of Archaean rocks of West Greenland. In: Windley, B.F. (Ed.), The Early History of the Earth. Wiley and Sons, London.

Kennedy, C.S., Kennedy, G.C., 1976. The equilibrium boundary between graphite and diamond. Journal of Geophysical Research 81, 2467–2470.

Kopylova, M.G., Russell, J.K., Cookenboo, H., 1999. Petrology of peridotite and pyroxenite xenoliths from the Jericho kimberlite: implications for the thermal state of the mantle beneath the Slave craton, Northern Canada. Journal of Petrology 40, 79–104.

Larsen, L.M., Rex, D.C., 1992. A review of the 2500 Ma span of alkaline-ultramafic, potassic and carbonatitic magmatism in West Greenland. Lithos 28, 367–402.

McKenzie, D., Priestley, K., 2008. The influence of lithospheric thickness variations on continental evolution. Lithos 102, 1–11.

McKenzie, D., Jackson, J., Priestley, K., 2005. Thermal structure of oceanic and continental lithosphere. Earth and Planetary Science Letters 233, 337–349.

Nickel, K.G., Green, D.H., 1985. Empirical geothermobarometry for garnet peridotites and implications for the nature of the lithosphere, kimberlites and diamonds. Earth and Planetary Science Letters 73, 158–170.

Nielsen, T.F.D., Sand, K.K., 2008. The Majuagaa kimberlite dike, Maniitsoq region, West Greenland: constraints on an Mg-rich silicocarbonatitic melt composition from groundmass mineralogy and bulk compositions. Canadian Mineralogist 46, 1043–1061.

Nielsen, T.F.D., et al., 2009, this issue. Distribution of kimberlite and aillikite in the Diamond Province of southern West Greenland: A regional perspective based on groundmass mineral chemistry and bulk compositions. Proceedings of the 9th International Kimberlite Conference. Lithos 112S, 358–371.

Nimis, P., Taylor, W.R., 2000. Single clinopyroxene thermobarometry for garnet peridotites. Part I. Calibration and testing of a Cr-in-Cpx barometer and an enstatite-in-Cpx thermometer. Contributions to Mineralogy and Petrology 139, 541–554.

O`Neill, H.S.C., Wood, B.J., 1979. Experimental-study of Fe–Mg partitioning between garnet and olivine and its calibration as a geothermometer. Contributions to Mineralogy and Petrology 70, 59–70.

Pearson, D.G., 2003. Mantle samples included in volcanic rocks: xenoliths and diamonds. In: Carlson, R.W. (Ed.), Treatise on geochemistry. Elsevier.

Pearson, D.G., Nowell, G.M., 2002. The continental lithospheric mantle reservoir: characteristics and significance as a mantle reservoir. Proceedings of the Royal Society, Series A 360, 1–28.

Pearson, D.G., Wittig, N., 2008. Formation of Archaean continental lithosphere and its diamonds: the root of the problem. Journal of the Geological Society 165, 895–914.

Pearson, N.J., Griffin, W.L., Doyle, B.J., O'Reilly, S.Y., van Achterbergh, E., Kivi, K., 1999. Xenoliths from kimberlite pipes of the Lac de Gras area, Slave Carton, Canada. In: Gurney, J.J., Gurney, J.L., Pascoe, M.D., Richardson, S.H. (Eds.), Proceedings of the VIIth International Kimberlite Conference. Red Roof Design cc, Cape Town, pp. 644–658.

Pollack, H.N., Chapman, D.S., 1977. Regional variation of heat-flow, geotherms, and lithospheric thickness. Tectonophysics 38, 279–296.

Rudnick, R.L., Nyblade, A.A., 1999. The thickness and heat production of Archean lithosphere: constraints from xenolith thermobarometry and surface heatflow. In: Yingwei Fei, Constance M Berkta and B. Mysen. (Editors), Mantle petrology: field observations and high pressure experiments: a tribute to Francis R (Joe) Boyd. Special Publication. The Geochemical Society.

Sand, K.K., 2007. A geotherm for the cratonic lithospheric mantle in southern West Greenland: thermal implications for diamond potential, Unpublished Masters thesis, University of Copenhagen.

Schulze, D.J., 2003. A classification scheme for mantle-derived garnets in kimberlite: a tool for investigating the mantle and exploring for diamonds. Lithos 71, 195–213.

Secher, K., Larsen, L.M., 1978. A new Phanerozoic carbonatite complex in southern West Greenland. Rapport Grønlands Geologiske Undersøgelse 90, 46–50.

Secher, K., Larsen, L.M., 1980. Geology and mineralogy of the Sarfartôq carbonatite complex, southern West Greenland. Lithos 13, 199–212.

Secher, K., et al., 2009, this issue. Timing of kimberlite, carbonatite, and ultramafic lamprophyre emplacement in the alkaline province located 64°–67° N in southern West Greenland. Proceedings of the 9th International Kimberlite Conference. Lithos 112S, 400–406.

Simon, N.S.C., Irvine, G.J., Davies, G.R., Pearson, D.G., Carlson, R.W., 2003. The origin of garnet and clinopyroxene in "depleted" Kaapvaal peridotites. Lithos 71, 289–322.

Smith, D., 1999. Temperatures and pressures of mineral equilibration in peridotite xenoliths: review, discussion, and implications. In: Yingwei Fei, Constance M Berkta and B. Mysen. (Editors), Mantle petrology: field observations and high pressure experiments: a tribute to Francis R (Joe) Boyd. Special Publication, The Geochemical Society.

Tappe, S., Foley, S.F., Kjarsgaard, B.A., Romer, R.L., Heaman, L.M., Stracke, A., Jenner, G.A., 2008. Between carbonatite and lamproite-diamondiferous Torngat ultramafic lamprophyres formed by carbonate-fluxed melting of cratonic MARID-type metasomes. Geochimica et Cosmochimica Acta 72, 3258–3286.

van Gool, J.A.M., Kriegsman, L.M., Marker, M., Nichols, G.T., 1999. Thrust stacking in the inner Nordre Stromfjord area, West Greenland — significance for the tectonic evolution of the Palaeoproterozoic Nagssugtoqidian orogen. Precambrian Research 93, 71–86.

van Gool, J.A.M., Connelly, J.N., Marker, M., Mengel, F.C., 2002. The Nagssugtoqidian orogen of West Greenland: tectonic evolution and regional correlations from a West Greenland perspective. Canadian Journal of Earth Sciences 39, 665–686.

Vernon, R.H., 2004. A Practical Guide to Rock Microstructures. Cambridge University Press, Cambridge.

Webb, M., 2007. Re–Os isotope constraints on the age of the lithospheric mantle beneath Western Greenland. Unpublished Masters Thesis, University of Durham.

Wedepohl, K.H., Heinrichs, H., Bridgwater, D., 1991. Chemical characteristics and genesis of the quartz–feldspathic rocks in the Archaean crust of Greenland. Contributions to Mineralogy and Petrology 107, 163–179.

Wittig, N., Pearson, D.G., Webb, M., Ottley, C.J., Irvine, G.J., Kopylova, M., Jensen, S.M., Nowell, G.M., 2008. Origin of cratonic lithospheric mantle roots: a geochemical study of peridotites from the North Atlantic Craton, West Greenland. Earth and Planetary Science Letters 274, 24–33.